Biosensors and Bioelectronics 131 (2019) 67–73

Contents lists available at ScienceDirect

Biosensors and Bioelectronics

journal homepage: www.elsevier.com/locate/bios

A sensitive sandwich-type immunosensor for the detection of MCP-1 based on a rGO-TEPA-Thi-Au nanocomposite and novel RuPdPt trimetallic nanoalloy particles

Weiran Mao[1], Junlin He[1], Zhiyong Tang, Chengli Zhang, Jun Chen, Jia Li, Chao Yu*

College of Pharmacy, Institute of Life Science and School of Public Health, Chongqing Medical University, Chongqing 400016, PR China

ARTICLE INFO

Keywords:
Immunosensor
Monocyte chemoattractant protein-1
Tetraethylene
Thionine
Trimetallic nanoalloy particles

ABSTRACT

A novel electrochemical immunosensor was proposed for the detection of monocyte chemoattractant protein-1 (MCP-1), a biomarker of cardiovascular disease. Due to thionine (Thi) possessing electroactive redox properties, a one-step approach was utilized to synthesize a reduced graphene oxide-tetraethylene-thionine-Au (rGO-TEPA-Thi-Au) nanocomposite at room temperature using the synergistic effect of Thi and rGO-TEPA towards $HAuCl_4$. We obtained the excellent matrix material, which immobilized more primary antibody MCP-1-Ab_1 on rGO-TEPA on a modified glassy carbon electrode (GCE). To further enhance the sensitivity of the sensor, a novel signal generation and amplification strategy was developed for detection. RuPdPt trimetallic nanoalloy particles (RuPdPt TNPs), a novel nanomaterial, were synthesized by a one-pot method, displayed a uniform morphology as well as good electrochemical activity and bound with the secondary antibodies against MCP-1 via the Pt-NH_2 bond. Most importantly, RuPdPt TNPs have a significant ability to catalyze H_2O_2 to produce an electron. The electrochemical signal was highly amplified because the electrochemical signal was primarily derived from the synergistic catalysis of H_2O_2 by RuPdPt TNPs and recorded by chronoamperometry. Under the optimal conditions, this newly designed biosensor exhibited sensitive detection of MCP-1 in the range from 20 fg mL^{-1} to 1000 pg mL^{-1}, with a detection limit of 8.9 fg mL^{-1} (based on a S/N = 3). Additionally, the designed immunosensor showed acceptable selectivity, reproducibility and stability. This immunosensor is a promising strategy for analyzing clinical serum samples in the future.

1. Introduction

Cardiovascular disease is the most common cause of death in developed countries, with 50% of the population dying from cardiovascular disease. Atherosclerosis is the main cause of cardiovascular disease (Walker, 2013). Monocyte chemoattractant protein-1 (MCP-1) is a member of the cysteine-cysteine family, also known as cysteine-cysteine chemokine ligand 2, which has a close relationship with the pathogenesis of cardiovascular disease (Gosling et al., 1999; Jacobson et al., 2000). The elevated levels of MCP-1 in human serum can lead to the development of atherosclerotic diseases such as unstable angina, myocardial infarction, and in-stent restenosis (Hartung et al., 2007; Montgomery and Brown, 2013). Therefore, measuring MCP-1 in serum is of great significance for the diagnosis and prediction of atherosclerotic diseases (McDermott et al., 2005; Nishiyama et al., 1998; Oshima et al., 2001). The traditional methods for determining the MCP-1 concentration include enzyme-linked immunosorbent assay (ELISA) (Hayashi et al., 2006), immunohistochemistry (Hartung et al., 2007), western blot (Pervin et al., 1998), and immunocytochemistry (Paine et al., 1993). Although these techniques are both sensitive and effective, they still suffer from the disadvantages of being expensive, time-consuming, and having relatively complex inspections. Therefore, an alternative approach for the sensitive detection of MCP-1 is urgently needed. An alternative for the quantitative analysis of MCP-1 is an electrochemical immunosensor, which has many advantages over traditional methods of detection, including simple operation, fast detection and low detection cost. However, electrochemical immunosensors also have the disadvantage that small current signals do not meet the required sensitivity, while higher sensitivity allows us to obtain accurate results with fewer biological samples. Therefore, we tend to establish sandwich immunosensors to improve the sensitivity of detection, and the signal amplification strategy is the key problem to be

* Correspondence to: College of Pharmacy, Chongqing Medical University, 1 Yi Xue Yuan Road, Box 380, Chongqing 400016, PR China.
E-mail address: yuchao@cqmu.edu.cn (C. Yu).
[1] These authors equally to this work.

https://doi.org/10.1016/j.bios.2019.02.021
Received 28 October 2018; Received in revised form 10 December 2018; Accepted 5 February 2019
Available online 19 February 2019
0956-5663/

solved by our new electrochemical immunosensor (Yuan et al., 2015).

Nanocomposites or hybrid materials have stimulated intense research over past decades due to their potential applications for bioassays. A novel material, reduced graphene oxide-tetraethylenepentamine (rGO-TEPA), not only has the overall properties of rGO (Wu et al., 2015) but also has many advantages over other carbon materials, such as substantial solubility and a large surface area (Guo et al., 2015; Wu et al., 2014). Most importantly, rGO-TEPA contains a large amount of amino groups, and it can easily combine with metal or biological materials to form a multifunctional nanocomposite. In order to immobilize antibodies on a rGO-TEPA-based electroactive nanocomposite, we use a one-step approach combining the synergistic effect of thionine (Thi) and rGO-TEPA towards $HAuCl_4$ to synthesize a rGO-TEPA-Thi-Au nanocomposite at room temperature (RT). The positively charged Thi molecule increases the adsorption capacity of the negatively charged $AuCl^{4-}$ ions. Moreover, the Thi molecules adsorbed on the nanocomposite still retain their electroactive redox properties (Liu et al., 2009). In addition, AuNPs in nanocomposites can provide active sites to immobilize biomolecules to prepare immunosensors. Finally, this nanocomposite can easily form a stable film having excellent conductivity on a glassy carbon electrode (GCE). Electrodes modified with this nanocomposite have better conductivity and thus achieve preliminary signal amplification.

The development of new signal materials is a core component of electrochemical immunosensor signal amplification. Recently, trimetallic nanocatalytic materials have attracted more attention than their single metal and bimetallic counterparts. Compared with bimetallic and single metal catalytic materials, trimetallic nanomaterials have better properties, such as chemical stability, a high surface area and fast electron transfer (Chopra et al., 2007; Wang, 2005). These properties occurred due to the combination of geometrical and electronic effects of the composite. These two effects simultaneously present and produce a synergistic effect on the catalytic activity in trimetallic catalysts, which is important for electrical analysis applications (Gao and Goodman, 2012). Here, the ruthenium palladium platinum trimetallic nanoalloy particles (RuPdPt TNPs) first synthesized by us were an ideal signal amplification label for detecting MCP-1. The main reasons are the following: first, the RuPdPt TNPs have the characteristics of a large surface area, uniform particle size and good electrical conductivity. Second, in the research on this subject, compared with traditional nanomaterials such as Pt nanoparticles and PdPt bimetallic nanoparticles, RuPdPt TNPs have strong catalytic activity. Finally, this material is capable of immobilizing biomolecules in large quantities via Pt-NH_2 bonds. In summary, the signal is greatly amplified by the catalysis of H_2O_2 by RuPdPt TNPs.

In this study, RuPdPt TNPs as a signal material and the rGO-TEPA-Thi-Au nanocomposite as an electrode modification material were synthesized, respectively. An ultrasensitive sandwich electrochemical immunosensor was designed for the high sensitivity quantitative detection of MCP-1. The rGO-TEPA-Thi-Au nanocomposite-modified electrode has excellent electrical conductivity and a larger specific surface area, and the primary antibody against MCP-1 (MCP-1-Ab_1) can bind to the material through the Au-NH_2 bond. In order to achieve the ultra-sensitive detection of targets, we introduced RuPdPt TNPs as a signal probe. As far as we know, this is the first report on the synthesis of RuPdPt TNPs for use in electrochemical sensors. Based on the above reasons, we have successfully prepared an ultrasensitive sandwich biosensor for MCP-1 detection (Scheme 1). At the same time, the experimental results indicated that the sensor exhibited acceptable selectivity, good reproducibility and desirable stability for MCP-1 detection, which will be promising for the diagnosis and prognosis of cardiovascular disease.

2. Experimental

2.1. Chemicals and materials

The human monocyte chemotactic protein-1 (MCP-1) ELISA Kit and monoclonal antibody to monocyte chemotactic protein-1 (MCP-1) were purchased from Cloud-Clone Corp. (St. Houston, USA, www.cloud-clone.com). Reduced graphene oxide-tetraethylenepentamine (rGO-TEPA) was obtained from the Nanjing XFNANO Materials Tech Co., Ltd. (China). Bovine serum albumin (BSA), potassium ferricyanide ($K_3Fe(CN)_6$) and potassium ferrocyanide ($K_4Fe(CN)_6$) were provided by the Beijing Chemical Reagents Company (Beijing, China). Pluronic F-127, gold (III) chloride trihydrate ($HAuCl_4{\cdot}4H_2O$) and ascorbic acid ($C_6H_6O_8$) were obtained from Sigma-Aldrich (Beijing, China). Sodium tetrachloropalladate (II) (Na_2PdCl_4) was obtained from the Shanghai Yuanye Bio-Technology Co., Ltd (Shanghai, China). Potassium tetrachloroplatinate (I) (K_2PtCl_4) was obtained from the Shanghai Macklin Biochemical Co., Ltd (Shanghai, China). Ruthenium (III) chloride anhydrous ($RuCl_3$) was obtained from the Shanghai Aladdin Bio-Chem Technology Co., Ltd (Shanghai, China). Dopamine (DA), L-cysteine, ascorbic acid (AA) and glucose were purchased from Aladdin (Shanghai, China, www.aladdin-e.com). Thionin was obtained from the Alfa Aesar Chemical Co. Ltd. (China). Doubly-distilled water was obtained from a Millipore Milli-Q purification system. The other chemicals were of analytical grade and used without further purification.

2.2. Apparatus and characterization

All electrochemical experiments were performed with a PARSTAT 4000+ electrochemical workstation (Princeton Application research, www.ameteksi.com). A conventional three electrode system was used for all electrochemical measurements, consisting of a platinum wire electrode as the counter electrode, a saturated calomel electrode (SCE) as the reference electrode, and a modified glassy carbon electrode (GCE, 4 mm in diameter) as the working electrode. The images of different nanomaterials were characterized by scanning electron microscopy (SEM, S-4800, Hitachi, Tokyo, Japan) at an acceleration voltage of 5.0 kV. Field emission scanning electron microscopy (FE-SEM) images were obtained using a Hitachi S4800 (Hitachi Limited, Japan). X-ray photoelectron spectroscopy (XPS) was implemented using a VG Scientific ESCALAB 250 spectrometer (Thermoelectricity Instruments, USA) with Al Kα X-ray radiation (1486.6 eV) as the light source. Fourier transform infrared (FT-IR) spectroscopy was performed with a Nicolet 6700 FT-IR spectrometer (Thermo Nicolet, USA). Energy dispersive X-ray spectroscopy (EDS) was scaled using a JEOL JSM-6700F microscope (Japan). Atomic force microscopy (AFM) images were monitored by Bruker Dimension Icon (USA).

2.3. Preparation of the rGO-TEPA-Thi-Au nanocomposite

RGO-TEPA-Thi-Au nanocomposites have been modified in previous literature by a simple one-step synthesis (Scheme 1A) (Han et al., 2013). Briefly, 3 mL of rGO-TEPA solution (1 mg mL^{-1}) was treated with ultrasound for at least 30 min first. Then, 3 mL of Thi (0.5 mM) and 25 μL of a 1% $HAuCl_4$ solution were added to the rGO-TEPA solution and stirred vigorously for 12 h at RT under dark conditions. The resulting nanocomposite was then collected by centrifugation at 9000 rpm for 15 min and washed three times with ultrapure water. Finally, the resulting precipitate was stored in 4 °C when not in use.

2.4. Preparation of RuPdPt TNPs, PdPt nanoparticles and Pt nanoparticles

An aqueous solution (2 mL) that contained K_2PtCl_4 (17.5 mM), Na_2PdCl_4 (2.5 mM), $RuCl_3$ (1.25 mM) and Pluronic F-127 (20 mg) was placed in a small beaker, and then AA (2 mL, 0.1 M) was quickly added under stirring. The final Pluronic F127 concentration was 0.397 mM.

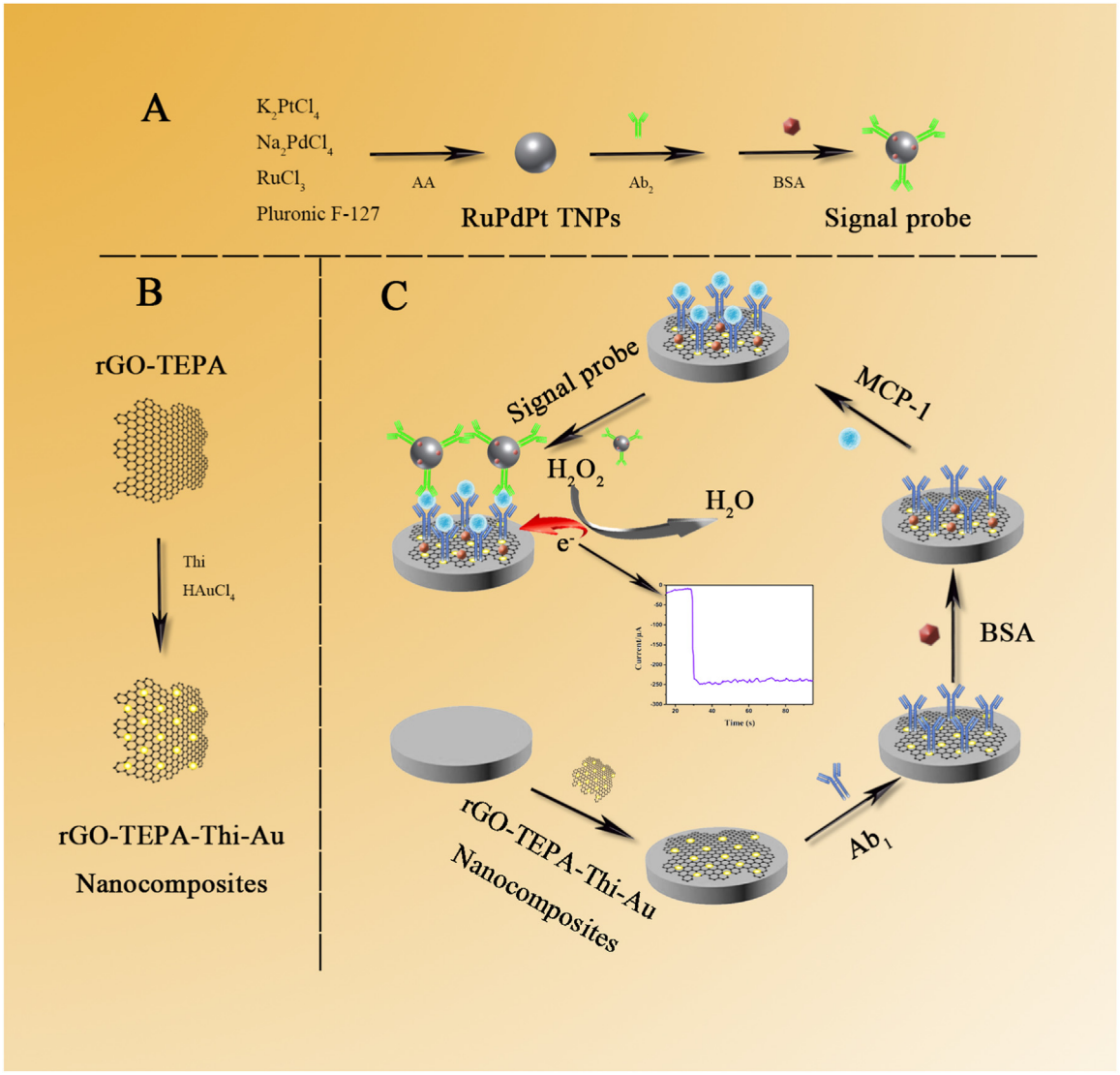

Scheme 1. The preparation procedures of the (A) signal probe and (B) rGO-TEPA-Thi-Au nanocomposite. (C) Schematic illustration of the stepwise assembly procedure of the electrochemical immunosensor interface.

The solution was stirred for 120 min at RT. The product was isolated and residual Pluronic F127 was removed after 120 min of reaction by centrifugation at 8000 rpm for 5 min, followed by consecutive washing/centrifugation cycles three times with ultrapure water. The collected product was lyophilized and stored in 4 °C when not in use. The PdPt nanoparticles and Pt nanoparticle composites were synthesized by a similar method (Wang and Yamauchi, 2010), except that we only used the same amount of K_2PtCl_4 and Na_2PdCl_4 in the synthesis of PdPt nanoparticles and we only used the same amount of K_2PtCl_4 in the synthesis of Pt nanoparticles.

2.5. Preparation of the signal probe

Scheme 1A presents the preparation procedure of the signal probe. MCP-1 antibody was dissolved in PBS (pH = 7.4, 10 mL) to obtain a MCP-1-Ab_2 stock solution (10 μg mL^{-1}). The solution of MCP-1-Ab_2 (10 μg mL^{-1}, 50 μL) was added into the RuPdPt TNPs (4.0 mg mL^{-1}, 1.0 mL), dissolved and shook for 12 h at 4 °C. Next, 100 μL of BSA (0.25%, w/v) was added into the above solution to block the active sites. Subsequently, the resultant solution was centrifuged, thoroughly washed to remove the unbound antibodies, redispersed in ultrapure water, and then stored at 4 °C for further use.

2.6. Fabrication of the electrochemical immunosensor

The fabrication procedure of the electrochemical biosensor is outlined in Scheme 1C. Prior to the fabrication of the immunosensor, the GCE was polished repeatedly with 0.3 and 0.05 μm alumina slurries, followed by a thorough rinsing with ultrapure water. After successive washing ultrasonically in baths of ultrapure water, absolute alcohol and ultrapure water, the electrode was dried at RT. Then, 10 μL of rGO-TEPA-Thi-Au nanocomposite aqueous suspension (2 mg mL^{-1}) was cast onto the electrode surface. Next, 10 μL of the MCP-1-Ab_1 solution (10 μg mL^{-1}) was dropped onto the modified electrode surface and combined with AuNPs via Au-NH_2 bonds. The electrode was placed at 37 °C for 2.5 h to allow the MCP-1-Ab_1 to more efficiently bond with the Au nanoparticles. After that, the electrode was blocked with a BSA solution (0.25%, w/v) for 30 min at 37 °C to eliminate nonspecific binding sites between the analyte and electrode. Then, 8.0 μL of MCP-1 solution with a series of concentrations was added onto the as-prepared electrode surface for 2 h at 37 °C. Finally, 10 μL of the prepared signal probe was cast onto the electrode surface and incubated for another 1 h. After each step, the modified electrode was thoroughly cleaned with ultrapure water to remove unbound attachments and then dried in air. The obtained immunosensor was stored at 4 °C in a dry environment

prior to use for further measurements.

2.7. Measurement procedure

All electrochemical measurements were performed on a conventional three-electrode system with a GCE 4.0 mm in diameter, a saturated calomel electrode and a platinum wire electrode as the working, reference and auxiliary electrodes, respectively. A scanning potential of − 0.4 V was chosen for amperometric i-t measurement of the electrochemical immunosensor in order to reduce the background current and minimize the responses of common interfering substances. After the background current was stable, 2.0 mol L^{-1} (20 μL) H_2O_2 was injected into the stirred PBS (5 mL, pH = 7.4), and then, the amperometric i-t current curve was recorded.

3. Results and discussion

3.1. Characterization of the prepared nanomaterials

The morphologies of the rGO-TEPA-Thi-Au nanocomposite and RuPdPt TNPs were identified by FE-SEM and TEM. Since Thi molecules were adsorbed on the rGO-TEPA surface through π–π and electrostatic interactions, $AuCl_4^-$ ions were reduced by rGO-TEPA to form AuNPs, which were stabilized by the excess Thi molecules. On the other hand, the abundant amino groups on rGO-TEPA chemically bonded these AuNPs. Therefore, Fig. 1A and Fig. 1B show the typical structure of AuNPs with an average diameter of approximately 30 nm, which are dispersed on wrinkled rGO-TEPA. In addition, in the FT-IR spectra, the rGO-TEPA-Thi-Au nanocomposite (curve b) has a more obvious absorption peak at 3400 cm^{-1} than rGO-TEPA (curve a), which means that rGO-TEPA-Thi-Au nanocomposites are richer in amino groups due to the reaction with Thi (Fig. S3). In addition, we can see the obvious gold peak in the UV spectrum in Fig. S4. These results revealed that the rGO-TEPA-Thi-Au nanocomposite was successfully synthesized.

In addition, the SEM image of RuPdPt TNPs (Fig. 1C) and TEM image of RuPdPt TNPs (Fig. 1D) revealed their monodisperse spherical structure with a size of approximately 30 nm. To further monitor the formation of the RuPdPt TNPs, EDS and XPS characterizations were employed to analyze their detailed composition. Ru, Pd, and Pt elements were observed in the XPS spectrum (Fig. 1E) and EDS spectrum of RuPdPt TNPs (Fig. 1F). Furthermore, the zeta potentials of the nanomaterials were investigated. As shown in Fig. S6, the zeta potential of Pt nanoparticles was − 14.7 mV (curve a), the zeta potential of PdPt bimetallic nanoparticles was −18.8 mV (curve b), and the zeta potential of RuPdPt TNPs was − 38.7 mV (curve c). All of the above results indicate that the synthesis of RuPdPt TNPs is successful and stable.

3.2. Comparison of different electrode modification materials

We evaluated the properties of different electrode modification materials and the results are shown in detail in Supplementary information (S1).

3.3. Comparison of different signal amplification strategies

The electrochemical behaviors of different nanomaterials were compared by amperometric i-t curves. As shown in Fig. S7, PdPt nanoparticles (curve b) show a stronger catalytic ability than Pt nanoparticles (curve a). This result shows that the Pd-Pt bimetallic nanoparticles are superior to the Pt nanoparticles alone, which is consistent with previous reports (Huang et al., 2009; Yamauchi et al., 2007; Ye and Crooks, 2007; Yuan et al., 2010). After combining PdPt with Ru, the RuPdPt TNPs (curve c) show a stronger catalytic ability than curves a and b due to the strong Ru catalytic ability toward H_2O_2. These results demonstrated that the proposed signaling material used in this biosensor has the best catalytic ability compared with the other materials in this experiment.

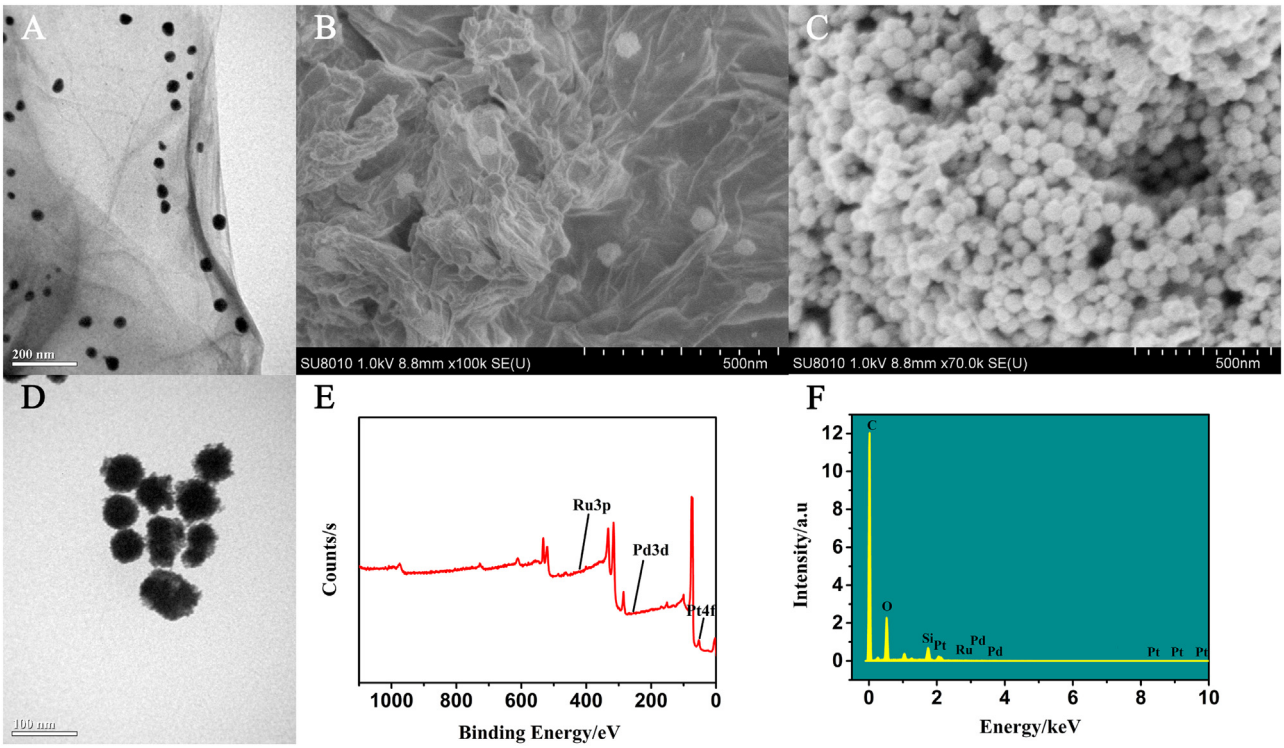

Fig. 1. (A) FE-TEM image of the rGO-TEPA-Thi-Au nanocomposite, (B) FE-SEM image of the rGO-TEPA-Thi-Au nanocomposite, (C) FE-TEM image of the RuPdPt TNPs, (D) FE-SEM image of the RuPdPt TNPs, (E) XPS of the RuPdPt TNPs, and (F) EDS spectrum of the RuPdPt TNPs.

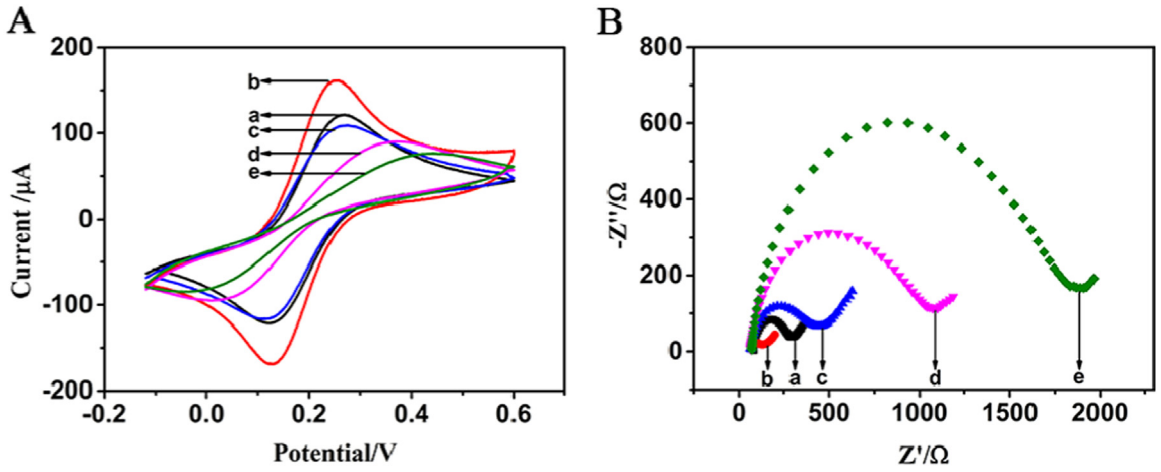

Fig. 2. CV (A) and EIS (B) of different modified electrodes in a 5 mM $Fe(CN)_6^{4-/3-}$ solution containing 0.1 M KCl: (a) bare GCE, (b) rGO-TEPA-Thi-Au/GCE, (c) Ab_1/rGO-TEPA-Thi-Au/GCE, (d) BSA/Ab_1/rGO-TEPA-Thi-Au/GCE and (e) target/BSA/Ab_1/rGO-TEPA-Thi-Au/GCE.

3.4. Electrochemical characterization of the stepwise modified electrodes

The step-by-step manufacturing process of the biosensor was characterized by CV and electrochemical impedance spectroscopy (EIS) in a 5 mM $[Fe(CN)_6]^{3-/4-}$ solution. The results of CV are shown in Fig. 2A, and the curve of the bare GCE (curve a) had a pair of typical reversible redox peaks. After the rGO-TEPA-Thi-Au nanocomposite was coated onto the electrode, the peak current was obviously increased (curve b) because of the excellent electrical conductivity of the rGO-TEPA-Thi-Au nanocomposite. After being combined with MCP-1-Ab_1 (curve c), BSA (curve d) and the target (curve e), a further decrease can be observed in the peak current because the bioactive substances greatly inhibited the efficiency of electron transfer.

The semicircle diameter of the electrochemical impedance spectroscopy (EIS) is equal to the electron transfer resistance (Ret), and the high frequency region of the impedance plot shows a semicircle related to the redox probe $[Fe(CN)_6]^{3-/4-}$. Therefore, the stepwise fabrication process was also monitored using EIS (Fig. 2B). It was found that the bare GCE produce a relatively small semicircle (curve a). When the electrode surface was modified by the rGO-TEPA-Thi–Au nanocomposite, the impedance value decreased (curve b), indicating that the rGO-TEPA-Thi-Au nanocomposite was conductive to the transmission of electrons. After the immobilization of the MCP-1-Ab_1, the semicircle diameter increased significantly (curve c). The resistance increased further when the nonspecific sites on the electrode surface were blocked with the non-conductive BSA (curve d). There was an apparent increase of resistance when the electrode was incubated with the target (curve e). The above phenomena are all due to the fact that biologically active substances greatly hinder the efficiency of electron transfer. All of the results obtained can be used to further support the successful fabrication of the constructed biosensor.

3.5. Optimization of the performance of the biosensor

The electrochemical properties of the immunosensor are influenced by many factors, and to enhance the catalytic efficiency and obtain a high sensitivity for the proposed electrochemical sensor, we choose to optimize several experimental conditions, and the results are shown in detail in Supplementary information (S2).

3.6. Analysis and detection

Under the optimal conditions, the fabricated sandwich-type electrochemical immunosensor was used to detect different concentrations of MCP-1 ranging from 20 ng mL^{-1} to 1000 pg mL^{-1}. As shown in Fig. 3A, the electrochemical signal gradually increased with increasing concentrations of MCP-1 in 5 mL of PBS (0.1 M, pH = 7.4). The calibration plots showed a strong linear dependence of current on the logarithm of the target concentration in the range from 20 fg mL^{-1} to 1000 pg mL^{-1}, with a detection limit of 8.9 fg mL^{-1} (based on S/N = 3), and the results are shown in Fig. 3B. The regression equation was Y = 87.11 + 42.51*X, with a correlation coefficient of 0.99673.

The excellent performance of the fabricated immunosensor may be ascribed to several factors. First of all, the rGO-TEPA-Thi-Au nanocomposite could promote the electron transfer and improve the immobilization of MCP-1-Ab_1. In addition, RuPdPt TNPs have excellent catalytic performance for H_2O_2 reduction, and the developed immunosensor showed a lower detection limit (Table 1). As a result, a novel and ultrasensitive immunosensor for MCP-1 detection was obtained.

3.7. Specificity, stability and reproducibility

To further test the nonspecific absorption of the other biological molecules on the immunosensor, control experiments have been performed by adding some interfering substances, such as AA, Glu, and BSA, instead of pure MCP-1. The current change of the immunosensor was recorded, and the results are depicted in Fig. 3C. Compared with pure MCP-1, the current response to each interferent was weak. The results suggest that the selectivity of the immunosensor was acceptable. To test the reproducibility of the electrodes, we measured each sample five times using five immunosensors prepared in parallel, and the peak current had no significant change (Fig. 3D), which demonstrates acceptable reproducibility. The rGO-TEPA-Thi-Au nanocomposite-modified immunosensor was stored in a refrigerator at 4 °C. The current change retained 85.2% of its original current change after storage for 21 days. This stability may be due to the good compatibility of the biomolecule with the substrate-modifying material.

3.8. Recovery testing

In order to verify the feasibility of the sensor in actual sample detection, the prepared immunosensor was used to detect the recovery of MCP-1 in the serum sample. The proposed electrochemical immunosensor was applied to human diluted serum samples spiked with 20 pg mL^{-1}, 200 pg mL^{-1} and 500 pg mL^{-1} MCP-1 antigen. The recoveries of the three concentrations were 101.9%, 99.4% and 101.2%, respectively (Table S1). The relative standard deviations of these three concentrations were 4.1%, 3.5% and 2.7%. In addition, compared to ELISA, the relative standard deviation between the two methods was

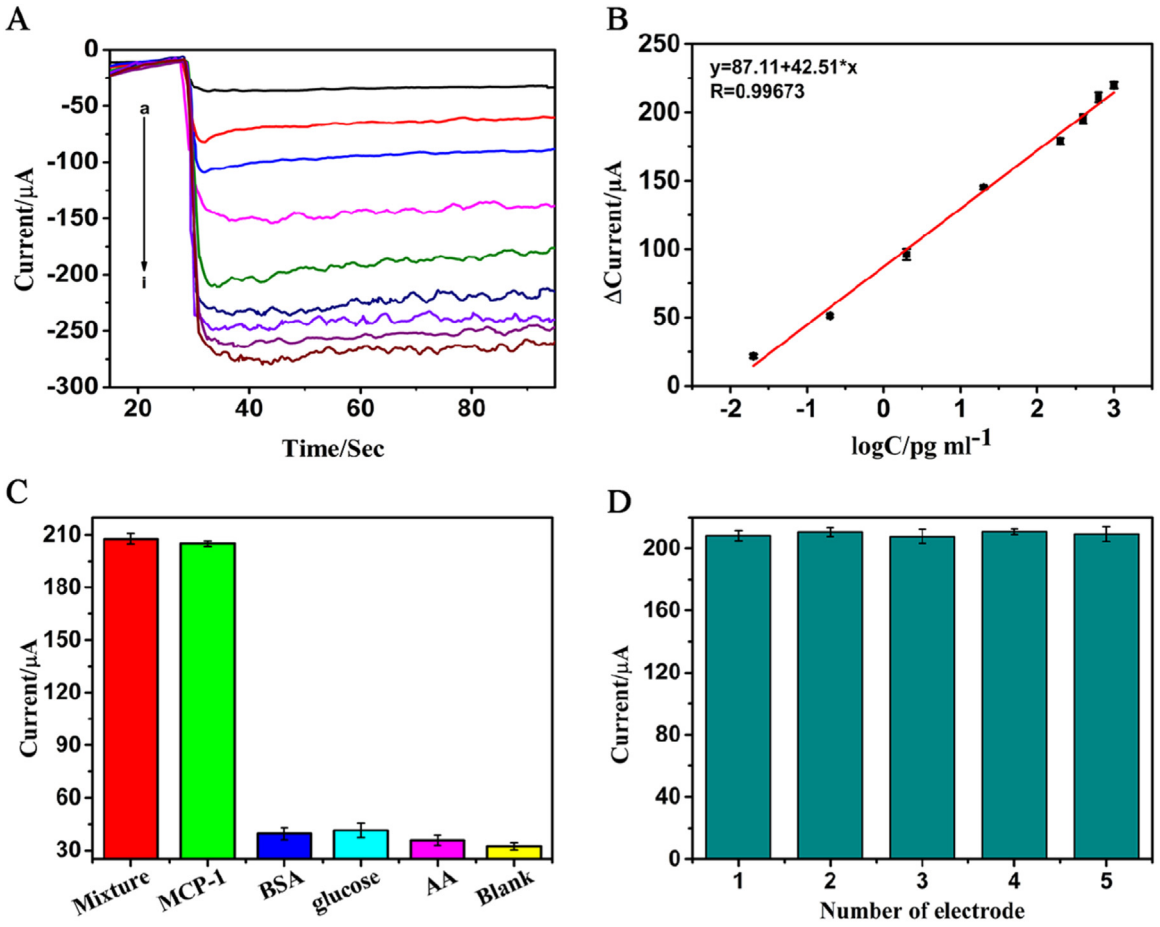

Fig. 3. (A) The i-t curve signals of the immunosensor for the determination of different concentrations of MCP-1: (a) 0, (b) 20 fg mL^{-1}, (c) 200 fg mL^{-1}, (d) 2 pg mL^{-1}, (e) 20 pg mL^{-1}, (f) 200 pg mL^{-1}, (g) 500 pg mL^{-1}, (h) 750 pg mL^{-1}, and (i) 1000 pg mL^{-1}. (B) The calibration curve of the immunosensor for different concentrations of MCP-1 (n = 3). (C) Specificity of the immunosensor towards the following analytes: 200 pg mL^{-1} MCP-1, AA, Glu, BSA and zero. (D) Reproducibility of 5 different electrodes modified with 200 pg mL^{-1} MCP-1.

from 1.8% to 5.6%, demonstrating little difference between the two assays (Table S2). These results indicate that our electrochemical immunosensors may provide a viable alternative for the determination of MCP-1 in human serum.

4. Conclusions

In this study, a specific sensitive sandwich electrochemical immunosensor based on a rGO-TEPA-Thi-Au nanocomposite and RuPdPt TNPs was successfully developed for the detection of MCP-1 in human serum. RGO-TEPA contains a large number of amino groups and significantly accelerates electron transfer. Thi molecules increase the adsorption capacity of negatively charged $AuCl^{4-}$ ions. AuNPs in the nanocomposite can provide active sites for immobilizing biological materials. In addition, RuPdPt TNPs have excellent catalytic properties for H_2O_2 reduction, and MCP-1-Ab_2 can be efficiently captured by Pt-NH_2. The developed sensor has a wide linear range with a low detection limit and a high specific interference in human serum as well as good reusability. In the follow-up experiments, we will try to shorten the construction time of the sensor and further improve the stability of the immunosensor to meet the requirements for the bedside detection of clinical markers.

Acknowledgements

We are grateful for the financial support from the National Natural Science Foundation of China (No. 81370403), the Chongqing Foundation and Advanced Research Project (No. CSTC2015jcyjBX0053), the Chongqing Precision Medical Key Technology Research and Development and Demonstration Projects (cstc2016shms-ztzx0042) and the Chongqing Medical University Scientific Research Cultivating Fund (No. 201414).

Declaration of interest statement

None.

Table 1
Comparing different methods for MCP-1 detection.

Detection methods	Liner range	LOD	Reference
sensors based on PIX-GrapheneAu-3 and MD/Graphene	1–100 pg mL^{-1}	1 pg mL^{-1}	(Stefan-van Staden et al., 2015)
Orderly oriented conductive wire-modified GCE	0.09–360 pg mL^{-1}	0.03 pg mL^{-1}	(Li et al., 2015)
Sandwich-type immunosensor based on a rGO-TEPA-Thi-Au nanocomposite and RuPdPt trimetallic nanoalloy particles	0.02–103 pg mL^{-1}	8.9 fg/mL	**This work**

Appendix A. Supplementary material

Supplementary data associated with this article can be found in the online version at doi:10.1016/j.bios.2019.02.021.

References

Chopra, N., Gavalas, V.G., Bachas, L.G., Hinds, B.J., Bachas, L.G., 2007. Anal. Lett. 40, 2067–2096.

Gao, F., Goodman, D.W., 2012. Chem. Soc. Rev. 41, 8009–8020.

Gosling, J., Slaymaker, S., Gu, L., Tseng, S., Zlot, C.H., Young, S.G., Rollins, B.J., Charo, I.F., 1999. J. Clin. Investig. 103, 773–778.

Guo, A., Li, Y., Cao, W., Meng, X., Wu, D., Wei, Q., Du, B., 2015. Biosens. Bioelectron. 63, 39–46.

Han, J., Ma, J., Ma, Z., 2013. Biosens. Bioelectron. 47, 243–247.

Hartung, D., Petrov, A., Haider, N., Fujimoto, S., Blankenberg, F., Fujimoto, A., Virmani, R., Kolodgie, F.D., Strauss, H.W., Narula, J., 2007. J. Nucl. Med. 48, 1816–1821.

Hayashi, M., Fujimoto, K., Urushibata, K., Takamizawa, A., Kinoshita, O., Kubo, K., 2006. Respirology 11, 24–31.

Huang, X., Zhang, H., Guo, C., Zhou, Z., Zheng, N., 2009. Angew. Chem. Int. Ed. Engl. 48, 4808–4812.

Jacobson, S.H., Thylen, P., Lundahl, J., 2000. Nephrol. Dial Transplant. 15, 1414–1419.

Li, Y., He, J., Xia, C., Gao, L., Yu, C., 2015. Biosens. Bioelectron. 70, 392–397.

Liu, H., Gao, J., Xue, M., Zhu, N., Zhang, M., Cao, T., 2009. Langmuir 25, 12006–12010.

McDermott, D.H., Yang, Q., Kathiresan, S., Cupples, L.A., Massaro, J.M., Keaney Jr., J.F., Larson, M.G., Vasan, R.S., Hirschhorn, J.N., O'Donnell, C.J., Murphy, P.M., Benjamin, E.J., 2005. Circulation 112, 1113–1120.

Montgomery, J.E., Brown, J.R., 2013. Vasc. Health Risk Manag. 9, 37–45.

Nishiyama, K., Ogawa, H., Yasue, H., Soejima, H., Misumi, K., Takazoe, K., Yoshimura, M., Kugiyama, K., Tsuji, I., Kumeda, K., 1998. Jpn. Circ. J. 62, 710–712.

Oshima, S., Ogawa, H., Hokimoto, S., Nakamura, S., Noda, K., Saito, T., Soejima, H., Takazoe, K., Ishibashi, F., Yasue, H., 2001. Jpn. Circ. J. 65, 261–264.

Paine 3rd, R., Rolfe, M.W., Standiford, T.J., Burdick, M.D., Rollins, B.J., Strieter, R.M., 1993. J. Immunol. 150, 4561–4570.

Pervin, S., Singh, R., Rosenfeld, M.E., Navab, M., Chaudhuri, G., Nathan, L., 1998. Arterioscler. Thromb. Vasc. Biol. 18, 1575–1582.

Stefan-van Staden, R.I., Gugoasa, L.A., Biris, A.R., 2015. Nanoscale 7, 14848–14853.

Walker, J., 2013. Nurs. Stand 28, 48–55.

Wang, J., 2005. Analyst 130, 421–426.

Wang, L., Yamauchi, Y., 2010. Chem. Asian J. 5, 2493–2498.

Wu, D., Guo, A., Guo, Z., Xie, L., Wei, Q., Du, B., 2014. Biosens. Bioelectron. 54, 634–639.

Wu, D., Guo, Z., Liu, Y., Guo, A., Lou, W., Fan, D., Wei, Q., 2015. Talanta 134, 305–309.

Yamauchi, Y., Ohsuna, T., Kuroda, K., 2007. Chem. Mater. 19, 1335.

Ye, H., Crooks, R.M., 2007. J. Am. Chem. Soc. 129, 3627–3633.

Yuan, G., Yu, C., Xia, C., Gao, L., Xu, W., Li, W., He, J., 2015. Biosens. Bioelectron. 72, 237–246.

Yuan, Q., Zhou, Z., Zhuang, J., Wang, X., 2010. Chem. Commun. 46, 1491–1493.